A correlation between the stellar and [Fe II] velocity dispersions in active galaxies

Rogemar A. Riffel,[1]⋆ Thaisa Storchi-Bergmann,[2] Rogério Riffel,[2] Miriani G. Pastoriza,[2] Alberto Rodríguez-Ardila,[3] Oli L. Dors Jr,[4] Jaciara Fuchs,[1] Marlon R. Diniz,[1] Astor J. Schönell Júnior,[1] Moiré G. Hennig[1] and Carine Brum[1]

[1]*Departamento de Física/CCNE, Universidade Federal de Santa Maria, 97105-900, Santa Maria, RS, Brazil*
[2]*Instituto de Física, Universidade Federal do Rio Grande do Sul, CP 15051, Porto Alegre 91501-970, RS, Brazil*
[3]*Laboratório Nacional de Astrofísica/MCT, Rua dos Estados Unidos 154, Itajubá, MG, Brazil*
[4]*Universidade do Vale do Paraíba, Av. Shishima Hifumi 2911, 12244-000, SŁo José dos Campos SP, Brazil*

ABSTRACT

We use near-infrared (near-IR) spectroscopic data from the inner few hundred parsecs of a sample of 47 active galaxies to investigate possible correlations between the stellar velocity dispersion ($\sigma_\star$), obtained from the fit of the K-band CO stellar absorption bands, and the gas velocity dispersion (σ), obtained from the fit of the emission-line profiles of [S III] $\lambda 0.953\,\mu$m, [Fe II] $\lambda 1.257\,\mu$m, [Fe II] $\lambda 1.644\,\mu$m and H$_2$ $\lambda 2.122\,\mu$m. While no correlations with $\sigma_\star$ were found for H$_2$ and [S III], a good correlation was found for the two [Fe II] emission lines, expressed by the linear fit $\sigma_\star = 95.4 \pm 16.1 + (0.25 \pm 0.08) \times \sigma_{[Fe II]}$. Excluding barred objects from the sample, a better correlation is found between $\sigma_\star$ and $\sigma_{[Fe II]}$, with a correlation coefficient of $R = 0.80$ and fitted by the following relation: $\sigma_\star = 57.9 \pm 23.5 + (0.42 \pm 0.10) \times \sigma_{[Fe II]}$. This correlation can be used to estimate $\sigma_\star$ in cases where it cannot be directly measured and the [Fe II] emission lines are present in the spectra, allowing us to obtain the mass of the supermassive black hole (SMBH) from the $M_\bullet$–$\sigma_\star$ relation. The scatter from a one-to-one relationship between $\sigma_\star$ and its value derived from $\sigma_{[Fe II]}$ using the equation above for our sample is 0.07 dex, which is smaller than that obtained in previous studies which use $\sigma_{[O III]}$ in the optical as a proxy for $\sigma_\star$. The use of $\sigma_{[Fe II]}$ in the near-IR instead of $\sigma_{[O III]}$ in the optical is a valuable option for cases in which optical spectra are not available or are obscured, as in the case of many active galactic nuclei. The comparison between the SMBH masses obtained using the $M_\bullet$–$\sigma_\star$ relation in which $\sigma_\star$ was directly measured with those derived from $\sigma_{[Fe II]}$ reveals only a small average difference of $\Delta \log M_\bullet = 0.02$ with a scatter of 0.32 dex for the complete sample and $\Delta \log M_\bullet = 0.00$ with a scatter of 0.28 dex for a subsample excluding barred galaxies.

Key words: black hole physics – galaxies: active – galaxies: nuclei – infrared: galaxies.

1 INTRODUCTION

In the present paradigm of galaxy evolution, most galaxies which form a bulge also form a supermassive black hole (SMBH) in their nuclei (e.g. Magorrian et al. 1998; Richstone et al. 1998; Ferrarese & Merrit 2000; Gebhardt et al. 2000). The central SMBH seems to play a fundamental role in the galaxy evolution, and cosmological simulations without considering the presence of a SMBH and its as-

sociated feedback predict masses for the galaxies much higher than those observed (Di Matteo, Springel & Hernquist 2005; Springel, Di Matteo & Hernquist 2005; Bower et al. 2006). In a scenario of co-evolution of the SMBH and its host galaxy, mass accretion to the central region of the galaxy leads to the growth of the galaxy bulge, while the feeding of the SMBH triggers episodes of nuclear activity which results in feedback in the form of radiation pressure and mass ejections from the accretion disc surrounding the SMBH. This episodic feedback may halt the mass accretion to the galaxy, preventing its growth in the active phase (Nemmen et al. 2007). This co-evolution may be the mechanism which leads to the empirical relation between the mass of the SMBH and the stellar

⋆ E-mail: rogemar@ufsm.br

velocity dispersion of the bulge, $M_\bullet$–$\sigma_\star$ (Ferrarese & Ford 2005; but see also Jahnke & Maccio 2011).

The $M_\bullet$–$\sigma_\star$ relation has been extensively used to estimate the mass of SMBHs from the stellar kinematics, as direct determinations of the SMBH masses are possible only for the closest galaxies for which the radius of influence of the SMBH can be resolved (e.g Ferrarese & Ford 2005). Although allowing us to estimate the masses of the SMBHs for a large number of galaxies, the use of the $M_\bullet$–$\sigma_\star$ relation requires the measurement of $\sigma_\star$, which is not always easy to obtain, particularly in active galaxies, where the active galactic nucleus (AGN) continuum dilutes the stellar absorption lines. In order to overcome this difficulty, a number of scaling relations using the width and luminosities of emission lines to determine $M_\bullet$ have been proposed (e.g. Nelson & Whittle 1996; Onken et al. 2004; Greene & Ho 2005, 2006; Kaspi et al. 2005; Salviander et al. 2006; Vestergaard & Peterson 2006; Peterson 2008; Wu 2009; Booth & Schaye 2011). Nevertheless, most of these relations are for the optical domain of the electromagnetic spectrum. With the improvement of infrared (IR) detectors, IR spectra of many AGNs have become recently available, and have the advantage of being less affected by reddening than optical spectra. In this paper, we investigate the possibility of using the widths of emission lines in the near-IR as proxies for $\sigma_\star$.

Recent studies by our group, using near-IR integral field spectroscopy of active galaxies, have allowed the mapping of the flux distributions and kinematics of the molecular (H_2) and ionized gas. We have found, in particular, that the H_2 usually shows small velocity dispersions and a velocity field dominated by rotation, while the ionized gas shows higher velocity dispersions and is not dominated by rotation (e.g. Riffel et al. 2006a, 2008, 2009; Storchi-Bergmann et al. 2009, 2010; Riffel, Storchi-Bergmann & Nagar 2010; Riffel & Storchi-Bergmann 2011a,b). The kinematics and flux distributions are also consistent with a location for the H_2 gas in the galaxy plane, while the ionized gas, and, in particular [Fe II], extends to high galactic latitudes.

In this paper, we investigate the correlation between the gas and stellar kinematics derived from near-IR spectroscopy, with the goal of looking for a 'proxy' for $\sigma_\star$ among the brightest emission lines in this wavelength range. This paper is organized as follows. In Section 2, we describe the sample and the observational data; in Section 3, we describe the methods used to measure the stellar and gaseous velocity dispersions. The results are presented in Section 4 and discussed in Section 5, while the conclusions are drawn in Section 6.

2 OBSERVATIONAL DATA

The spectroscopic data used in this work are from Riffel, Rodríguez-Ardila & Pastoriza (2006b), Rodríguez-Ardila, Contini & Viegas (2005) and Rodríguez-Ardila et al. (2004). The sample comprises 47 active galaxies with a range of activity types, and the spectra cover, on average, the inner 300 pc radius of the galaxies.

The near-IR spectra were obtained with the NASA 3-m Infrared Telescope Facility (IRTF), using the SpeX spectrograph in the short cross-dispersed mode (0.8–2.4 μm). The detector employed was a 1024 × 1024 ALADDIN 3 InSb array with a spatial scale of 0.15 arcsec pixel^{-1}. A 0.8 × 15 arcsec^2 slit was used and the spectral resolution is 300 km s^{-1}, obtained from the measurement of the full width at half-maximum of Arc lamp lines, or 127 km s^{-1} in σ. The data reduction followed standard procedures. For more details on the instrumental configuration, data reduction, calibration processes and details of the extraction of the spectra, see Riffel et al. (2006b).

The above sample was chosen for this work because it is a unique data set of near-IR spectroscopy of active galaxies, observed with the same instrumental setup (thus with no instrumental bias), covering the near-IR *Z, J, H* and *K* bands, and including several emission and absorption features allowing the comparison of the stellar and gas kinematics.

3 METHODS

In order to obtain the gaseous velocity dispersion σ, we fitted the emission-line profiles of [S III] $\lambda 0.953\,\mu m$, [Fe II] $\lambda 1.257\,\mu m$, [Fe II] $\lambda 1.644\,\mu m$ and H_2 $\lambda 2.122\,\mu m$ by single Gaussian curves and adopted as the measured velocity dispersion the σ of the Gaussian. These emission lines have been chosen because they are the strongest in the near-IR spectra of active galaxies (e.g. Riffel et al. 2006b). We excluded the H and He recombination lines due to uncertainties in the fit for type 1 objects, for which is not always easy to separate the narrow from the broad components. The fitting of the emission-line profiles was done by adapting the PROFIT routine (Riffel 2010), which outputs the emission-line flux, the centroid velocity, the velocity dispersion and the uncertainties for each of these parameters. The velocity dispersion was then corrected for the instrumental $\sigma_{inst} = 127$ km s^{-1}, which was subtracted in quadrature from the σ obtained from the fit of the Gaussians to the line profiles.

We measured the stellar velocity dispersion ($\sigma_\star$) using the PPXF (penalized Pixel-Fitting) method of Cappellari & Emsellem (2004) in order to fit the CO absorption bands at ∼2.3 μm in the *K* band. The PPXF method requires the use of stellar spectra as templates. We used for this the spectra of 60 late-type stars, 40 of them from the Gemini Near-IR Late-type stellar library (Winge, Riffel & Storchi-Bergmann 2009) and the remaining 20 spectra are from stars with public NIFS observations in the Gemini data archive (Diniz et al., in preparation). The uncertainties on the measurements of $\sigma_\star$ were estimated using 100 Monte Carlo iterations as in Riffel & Storchi-Bergmann (2011b).

In order to illustrate our procedures, we show in Fig. 1 sample fits of the CO absorption band heads at 2.3 μm using the PPXF method, as well as fits of the emission-line profiles using PROFIT for the spectrum of the galaxy NGC 5929.

4 RESULTS

The resulting measurements for the stellar and gas velocity dispersions for the galaxies of our sample are shown in Table 1. The dashes in the table are due to the fact that for a few objects we were not able to measure one or more values due to the absence of the absorption/emission lines or due to a low signal-to-noise ratio.

We have looked for correlations between the stellar and gaseous velocity dispersions using the values of Table 1 to construct the graphs of Figs 2, 3 and 4. We have used the IDL routine R_CORRELATE to obtain the Spearman correlation coefficient *R* for each graph. Fig. 2 shows $\sigma_\star$ versus σ_{H_2}. The range of the $\sigma_\star$ and σ_{H_2} values is approximately the same, something we have noticed in our previous studies of individual galaxies using integral field spectroscopy of the inner hundreds of parsecs (e.g. Riffel et al. 2008, 2009; Riffel & Storchi-Bergmann 2011a,b). Nevertheless, we have obtained only a very weak correlation between σ_{H_2} and $\sigma_\star$, with $R = 0.35$, but we note that the H_2 line is unresolved for several objects.

The relation between $\sigma_\star$ and $\sigma_{[Fe II]}$ is presented in Fig. 3, showing that $\sigma_{[Fe II]}$ is usually higher than $\sigma_\star$, which is also in agreement with
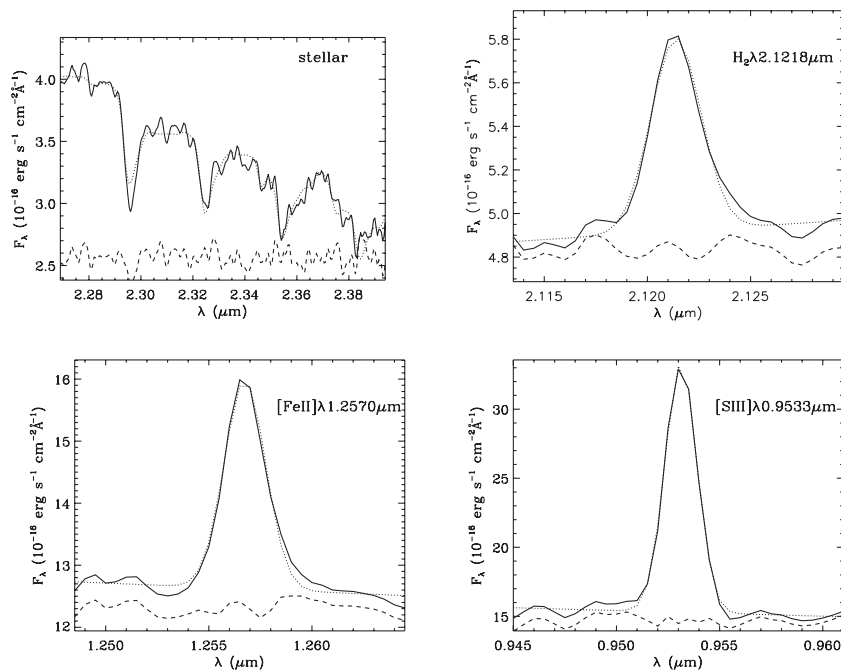
Figure 1. Sample fits of the spectrum of the galaxy NGC 5929. Top left-hand panel: fit of the stellar absorption spectra to obtain the stellar kinematics. Remaining panels: fit of the emission-line profiles of H_2, [Fe II] and [S III]. The observed spectra are shown as the continuous lines, the fits as the dotted lines and the residuals as the dashed lines.

the results from the integral field spectroscopic studies above. A better correlation is observed between $\sigma_\star$ and $\sigma_{[Fe II]}$ than with σ_{H_2}, corresponding to a correlation coefficient $R = 0.56$ obtained as described above. We fitted the data by a linear equation of the form $\sigma_\star = A + B \times \sigma_{[Fe II]}$ using the IDL routine LINMIX_ERR, which uses a Bayesian approach to linear regression with errors in both variables and takes into account upper limits for the measurements (Kelly 2007). The best fit to the data is given by

$$\sigma_\star = 95.4 \pm 16.1 + (0.25 \pm 0.08) \times \sigma_{[Fe II]} \tag{1}$$

which is shown as a dashed line in Fig. 3.

Finally, the relation between $\sigma_\star$ and $\sigma_{[S III]}$ is shown in Fig. 4, resulting in a correlation coefficient $R = 0.32$, suggesting only a very weak correlation. This figure also shows that $\sigma_{[S III]}$ is larger than $\sigma_\star$ by more than a hundred $km\,s^{-1}$, on average.

5 DISCUSSION

The use of the velocity dispersion from the narrow-line region emission lines as a proxy for $\sigma_\star$ in order to obtain an estimate for the SMBH mass via the M_{BH}–$\sigma_\star$ relation in active galaxies is not new. It has been previously used in the optical domain, where the emission line most commonly used is [O III] $\lambda5007\,\mu m$ (e.g. Onken et al. 2004; Kaspi et al. 2005; Salviander et al. 2006; Wu 2009). This emission line has been used instead of $\sigma_\star$ because in active galaxies $\sigma_\star$ cannot be easily measured due to dilution of the stellar absorption lines by the AGN continuum or its scattered light.

In this paper, we present an alternative to be used in the near-IR. As shown above, we found a correlation between $\sigma_\star$ and $\sigma_{[Fe II]}$, indicating that the latter can be used to estimate $\sigma_\star$ using equation (1). [Fe II] has two similarly strong emission lines which can be observed in the near-IR: [Fe II] $\lambda1.257\,\mu m$ in the J band and [Fe II] $\lambda1.644\,\mu m$ in the H band. In Fig. 5 we present a comparison between the σ of these two lines, where the solid line shows a

one-to-one relationship. This comparison shows that the width of these lines is the same within the errors, with a mean difference of $\sigma_{[Fe II]\lambda1.644} - \sigma_{[Fe II]\lambda1.257} = 8\ km\,s^{-1}$ and a scatter of $47\ km\,s^{-1}$, as seen in the top panel of Fig. 5. This scatter may be partially due to the fact that [Fe II] $\lambda1.644$ is close in wavelength to Brackett 12, which usually appears in absorption and may affect the measurement of the [Fe II] line.

Why is $\sigma_{[Fe II]}$ better correlated with $\sigma_\star$ than σ_{H_2}? As pointed out in the Introduction, our previous studies using integral field spectroscopy (Riffel et al. 2008, 2009; Riffel & Storchi-Bergmann 2011a,b) showed that the H_2 kinematics frequently show a rotation pattern and a smaller velocity dispersion than that of the ionized gas. This also led to the conclusion that the H_2 gas was more restricted to the galaxy plane, while the ionized gas – and in particular [Fe II] – extended to higher galactic latitudes. The integrated value of $\sigma_\star$ from the nuclear region of galaxies is dominated by the contribution of bulge stars, which are not restricted to the plane, showing 'hotter' kinematics. Thus, it can be understood that the velocity dispersion of gas which is restricted to the plane does not correlate with that of bulge stars, while that of gas extending to higher latitudes, similar to that of the bulge, such as the [Fe II] emitting gas, is correlated to that of the bulge stars. The higher values of $\sigma_{[Fe II]}$ relative to $\sigma_\star$ are probably due to extra heating provided by a nuclear AGN outflow.

Our results can be compared with previous ones in the optical using the σ of the [O III] $\lambda5007\,\mu m$ emission line as a proxy for $\sigma_\star$. For a sample of 66 Seyfert galaxies, Nelson & Whittle (1996) found a scatter of 0.20 dex around a one-to-one relation between $\sigma_\star$ and $\sigma_{[O III]}$, while Onken et al. (2004) found a smaller scatter of 0.15 dex for a sample of 16 AGNs, for which 25 per cent of their sources have $\sigma_{[O III]}$ deviating by more than 0.20 dex from the values expected based on their $\sigma_\star$. We found a scatter of 0.07 dex between the values obtained via equation (1) and the measured values for $\sigma_\star$, which is thus smaller than that for $\sigma_{[O III]}$.

Table 1. Stellar and gas velocity dispersions for the galaxies of the sample.

Object	Hubble type[a]	Nuclear activity[a]	$\sigma_\star$ (km s^{-1})	σ_{H_2} (km s^{-1})	$\sigma_{[Fe\,II]}$ (km s^{-1})	$\sigma_{[S\,III]}$ (km s^{-1})
Mrk 334	Sbc	Sy1	<127	<127	180 ± 9	278 ± 14
NGC 34	S0/a	Sy2	160 ± 23	198 ± 17	227 ± 19	215 ± 18
NGC 262	S0/a	Sy2	–	<127	263 ± 17	245 ± 16
Mrk 993	Sa	Sy2	132 ± 14	185 ± 10	214 ± 12	287 ± 16
NGC 591	SB0/a	Sy2	130 ± 21	<127	274 ± 17	229 ± 14
Mrk 573	SB0	Sy2	<127	<127	172 ± 12	211 ± 15
NGC 1097	SB(s)b	Sy1	165 ± 13	<127	166 ± 12	381 ± 28
NGC 1144	E	Sy2	206 ± 40	175 ± 13	230 ± 18	233 ± 18
Mrk 1066	S0/a	Sy2	<127	<127	206 ± 15	234 ± 17
NGC 1275	S0	Sy2	–	173 ± 21	313 ± 38	564 ± 68
NGC 1614	SB(s)c	Sb	<127	<127	203 ± 12	217 ± 13
MCG-5-13-17	SB0/a	Sy1	162 ± 11	191 ± 22	162 ± 19	201 ± 23
NGC 2110	E-S0	Sy2	184 ± 16	<127	248 ± 17	305 ± 21
ESO 428−G014	S0	Sy2	<127	161 ± 11	233 ± 18	253 ± 18
Mrk 1210	S?	Sy2	181 ± 24	<127	316 ± 32	342 ± 35
Mrk 124	S?	NLS1	222 ± 23	235 ± 27	335 ± 39	244 ± 29
Mrk 1239	E-S0	NLS1	–	–	<127	370 ± 35
NGC 3227	SB(s)a	Sy1	128 ± 3	157 ± 24	314 ± 48	276 ± 42
H1143−192	–	Sy1	–	–	170 ± 28	410 ± 68
NGC 3310	SB(r)bc	Sb	142 ± 18	<127	130 ± 9	153 ± 10
PG1126−041	S	QSO	–	<127	254 ± 34	363 ± 48
NGC 4051	SB(rs)bc	NLS1	<127	<127	142 ± 6	215 ± 9
NGC 4151	SB(rs)ab	Sy1	136 ± 19	<127	194 ± 41	231 ± 48
Mrk 766	SB(s)a	NLS1	<127	<127	133 ± 20	188 ± 19
NGC 4748	S?	NLS1	<127	170 ± 15	171 ± 21	273 ± 23
TONS0156	–	QSO	–	–	<127	712 ± 200
Mrk 279	S0	NLS1	138 ± 12	<127	209 ± 49	335 ± 79
NGC 5548	S0/a	Sy1	<127	<127	165 ± 43	213 ± 55
Mrk 478	Sc	NLS1	–	161 ± 22	171 ± 23	390 ± 53
NGC 5728	SBa	Sy2	<127	132 ± 23	<127	223 ± 38
PG1448+273	E?	QSO	–	<127	–	303 ± 1
Mrk 684	Sab	Sy1	170 ± 17	351 ± 18	–	540 ± 27
Mrk 291	SBa	NLS1	–	129 ± 14	144 ± 16	167 ± 18
Mrk 493	SBb	NLS1	–	<127	232 ± 12	412 ± 21
NGC 5929	Sa	Sy2	158 ± 23	<127	208 ± 26	181 ± 23
NGC 5953	S0/a	Sy2	149 ± 4	187 ± 8	289 ± 13	289 ± 13
PG1612+261	–	QSO	166 ± 18	–	266 ± 53	262 ± 52
Mrk 504	S?	NLS1	<127	<127	–	333 ± 38
3C351	–	BLRG	–	–	–	187 ± 14
ARP102B	E0	Sy1	<127	155 ± 9	195 ± 10	299 ± 16
1H 1934-063	–	NLS1	184 ± 9	191 ± 8	238 ± 11	291 ± 13
Mrk 509	E-S?	Sy1	<127	–	159 ± 39	370 ± 91
1H2107-097	–	Sy1	<127	–	<127	256 ± 56
Ark 564	Sbc	NLS1	–	180 ± 10	176 ± 10	260 ± 15
NGC 7469	SBbc	Sy1	–	–	161 ± 15	283 ± 18
NGC 7682	SBab	Sy2	183 ± 40	<127	198 ± 27	205 ± 28
NGC 7714	SB(s)b	H II	<127	<127	165 ± 13	184 ± 14

[a]The Hubble type and nuclear activity were taken from the NASA/IPAC Extragalactic Database (NED) and Hyperleda data base (Paturel et al. 2003).

A cautionary note is the observation of recent spatially resolved studies (e.g. our previous studies already mentioned) that the [Fe II] emission originates at least in part in outflowing gas. Thus, the width of the line is not only due to orbital motion in the gravitational potential of the galaxy, but also due to broadening by the outflow, what is consistent with the observation that $\sigma_{[Fe\,II]}$ is larger than $\sigma_\star$. Similar outflows – most probably the same – are observed in the [O III]-emitting gas (e.g. Das et al. 2005; Crenshaw & Kraemer 2007; Das, Crenshaw & Kraemer 2007; Crenshaw et al. 2009, 2010; Fischer et al. 2010, 2011). Nevertheless, this line has been frequently used as a proxy for $\sigma_\star$ as discussed above, due to the lack of a better indicator. Our argument is that $\sigma_{[Fe\,II]}$ is at least

as good a $\sigma_\star$ proxy as $\sigma_{[O\,III]}$, and can be used when the latter is not available.

We thus propose the use of $\sigma_{[Fe\,II]}$ to obtain $\sigma_\star$ via equation (1) in cases for which it is not possible to measure the stellar kinematics of the galaxy, and the optical spectrum is obscured or not available, so that the [O III] $\lambda 5007$ emission line is also not available. Nevertheless, this suggestion should be used with care, since the $M_\bullet$–$\sigma_\star$ relation is calibrated from a parent sample of mostly early-type galaxies and, as seen in Table 1, most of the objects of our sample are late type. Late-type galaxies can have distinct $\sigma_\star$ values from those of early-type galaxies, since the orbits of the stars in a disc are different from the orbits of the stars in the bulge. Additionally,
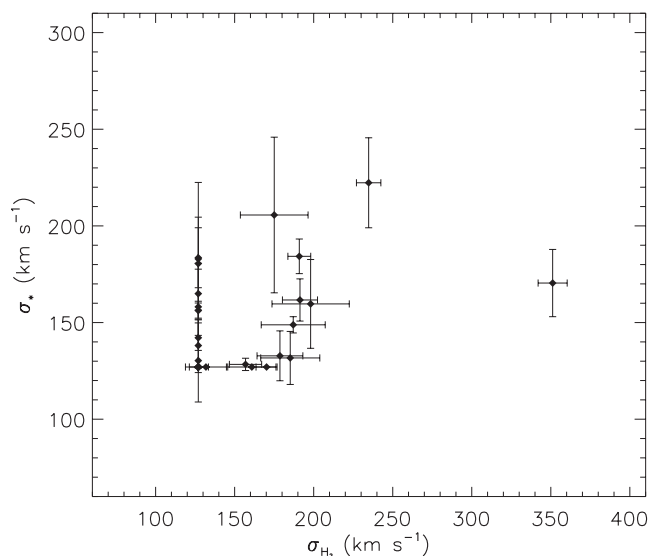
Figure 2. Comparison between the gas velocity dispersions obtained from the H_2 λ2.122 μm emission line (σ_{H_2}) and the stellar velocity dispersions from the CO stellar absorptions at ~2.3 μm ($\sigma_\star$). The points with no error bars in one or both axes represent measurements that are unresolved by our observations and should be considered as upper limits.
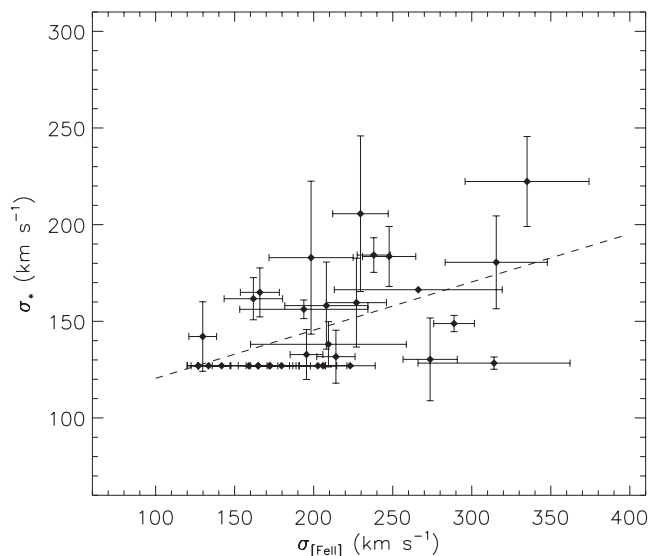

Figure 3. Same as Fig. 2 but for the gas velocity dispersion derived using [Fe II] λ1.257 μm. The dashed line represents the best linear fit of the data, given by: $\sigma_\star = 95.4 \pm 16.1 + (0.25 \pm 0.08) \times \sigma_{[Fe II]}$.

some of the galaxies of our sample have bars, circumnuclear star-forming rings or nuclear starbursts or even are classified as peculiar objects and thus the $\sigma_\star$ measured for these objects could be very different from those for the classical bulge, used to calibrate the $M_\bullet$–$\sigma_\star$ relationship.

5.1 The effect of galaxy morphology on the $M_\bullet$–σ relation

As pointed out above, the $M_\bullet$–$\sigma_\star$ relation is calibrated using a parent sample of mostly early-type galaxies. However, Table 1 shows that about 30 per cent of the galaxies of our sample are late type, which can have distinct $\sigma_\star$ values from those of early-type galaxies, since the orbits of the stars in a disc (which dominate in late-type galaxies)
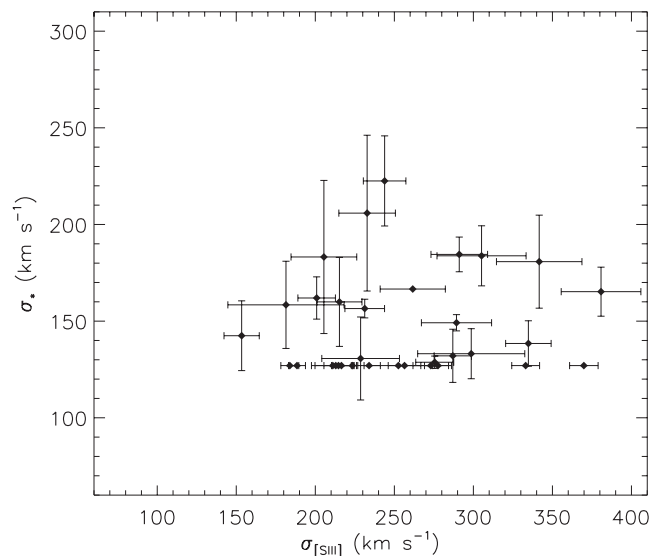

Figure 4. Same as Fig. 2 but for the gas velocity dispersion derived using [S III] λ0.953 μm.

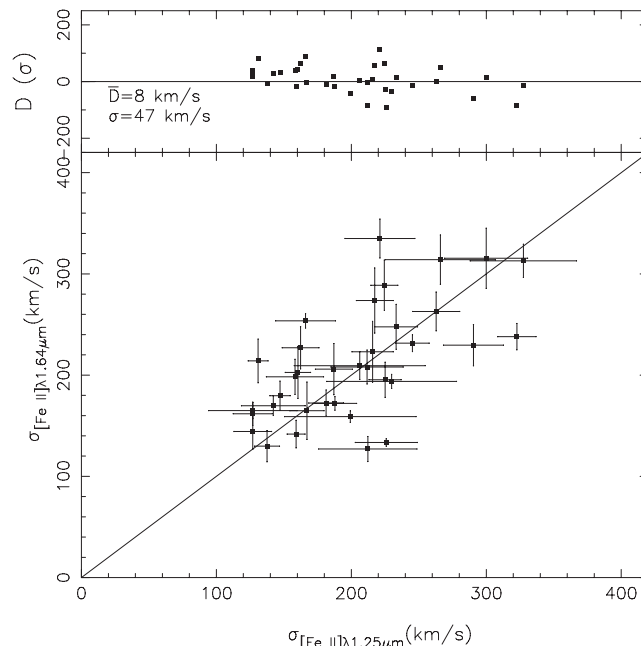**Figure 5.** $\sigma_{[Fe II]\lambda 1.644}$ versus $\sigma_{[Fe II]\lambda 1.257}$. The solid line represents a one-to-one relationship. The top panel shows the difference between the values of $\sigma_{[Fe II]\lambda 1.644}$ and $\sigma_{[Fe II]\lambda 1.257}$ defined as $D(\sigma) = \sigma_{[Fe II]\lambda 1.644} - \sigma_{[Fe II]\lambda 1.257}$, as well as the average value of this difference ($\bar{D}$).

are distinct from those in a bulge (which dominate in early-type galaxies). Additionally, ≈30 per cent of the galaxies of our sample have bars, and another 30 per cent have uncertain classifications and are peculiar objects which may not obey the the $M_\bullet$–$\sigma_\star$ relationship.

Xiao et al. (2011) investigated the $M_\bullet$–$\sigma_\star$ relation for late-type galaxies for a sample of 93 objects with a Seyfet 1 nucleus. They examined the $M_\bullet$–$\sigma_\star$ relationship for subsamples of barred and unbarred host galaxies and found no difference in slope. They only found a mild offset in the relation between low- and high-inclination disc galaxies, with the latter tending to have larger $\sigma_\star$ for a given value of the black hole mass.
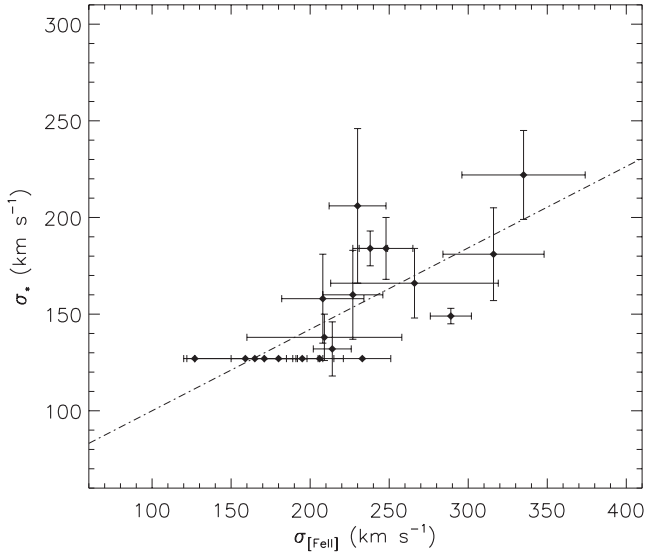
Figure 6. Same as Fig. 2 but for the gas velocity dispersion derived using [Fe II] $\lambda 1.257\,\mu$m for the subsample of unbarred galaxies. The dashed line represents the best linear fit of the data, given by: $\sigma_\star = 57.9 \pm 23.5 + (0.42 \pm 0.10) \times \sigma_{[Fe II]}$.

The $M_\bullet$–$\sigma_\star$ relationship for galaxies of different Hubble types have also been studied by Graham et al. (2011) using a sample of 64 galaxies. They found that restricting the sample only to elliptical galaxies, or only to non-barred galaxies, results in tighter relations (with less scatter) and a smaller slope than when using the full sample of galaxies. The $M_\bullet$–$\sigma_\star$ relation obtained when the sample is restricted to barred galaxies only lies ≈ 0.45 dex below the relation obtained for elliptical and non-barred galaxies.

In order to investigate the effect of the presence of a bar in the $M_\bullet$–$\sigma_{[Fe II]}$ relation of Fig. 3, we divided our sample into two subsamples: one composed of barred galaxies only and the other of unbarred galaxies. We found a much better correlation between $\sigma_{[Fe II]}$ and $\sigma_\star$ for the unbarred galaxies than for the total sample, as illustrated in Fig. 6. The correlation coefficient is $R = 0.80$ and a linear regression to the relation is given by

$$\sigma_\star = 57.9 \pm 23.5 + (0.42 \pm 0.10) \times \sigma_{[Fe II]}. \qquad (2)$$

On the other hand, no correlation was found for the barred galaxies, for which the correlation coefficient between $\sigma_{[Fe II]}$ and $\sigma_\star$ is only $R = 0.20$.

Approximately half of our sample is composed of early-type galaxies (half of which are barred), the remainder being late-type galaxies and galaxies with uncertain morphology (usually because they are distant and compact). However, the number of galaxies of our sample is not large enough to further investigate the effect of morphology (besides the effect of bars discussed above) on the $\sigma_\star$–$\sigma_{[Fe II]}$ relation. This will be possible only when more near-IR AGN spectra become available, and equations (1) and (2) could be better calibrated using large non-biased samples of galaxies.

On the other hand, when applying the $\sigma_\star$–$\sigma_{[Fe II]}$ relation to distant galaxies, it will be hard to ascertain a Hubble type to such galaxies, and it will probably be better to just use the relation for the whole sample (equation 1), despite the fact that a relation for restricted Hubble types (e.g. for galaxies without bars) shows less scatter.

Many present/future missions are discovering/will discover large numbers of obscured AGNs, such as the *WISE* mission
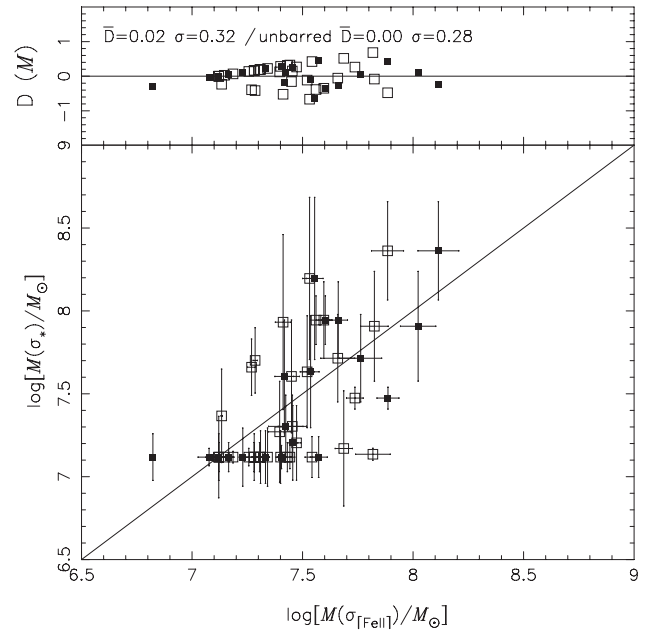

Figure 7. Comparison between SMBH mass values obtained directly from the relation with $\sigma_\star$ (*y*-axis) and using $\sigma_{[Fe II]}$ (*x*-axis) to obtain $\sigma_\star$. The filled squares are for the complete sample, for which equation (1) was used, and the open squares for unbarred galaxies, for which equation (2) was used. The error bars shown include the uncertainties in the calibration of the $M_\bullet$–$\sigma_\star$ relation.

(http://www.nasa.gov/mission_pages/WISE/news/wise201 20829.html) or the VISTA Variables in The Via Lactea survey (http://mwm.astro.puc.cl/mw/index.php/Main_Page), which are potential samples to benefit from the relation we have found in order to obtain the SMBH masses, if [Fe II] emission lines are present in the spectra.

5.2 Estimating SMBH masses using $\sigma_{[Fe II]}$

We now evaluate the effect of the scatter introduced by the use of equation (1) in the value of SMBH masses obtained via the $M_\bullet$–$\sigma_\star$ relation, which result in higher uncertainties in $M_\bullet$ than those obtained by using $\sigma_\star$ directly. In order to do this, we use the relation below from Graham et al. (2011):

$$\log(M_\bullet/M_\odot) = (8.13 \pm 0.05)$$
$$+ (5.13 \pm 0.34) \log[\sigma_\star/200\,\mathrm{km\,s}^{-1}] \qquad (3)$$

to obtain $M_\bullet/M_\odot$, using for $\sigma_\star$ first its measurement from the stellar kinematics and then the value derived from $\sigma_{[Fe II]}$ using equation (1). We compare the two values in Fig. 7 [log $M(\sigma_\star)$ versus log $M(\sigma_{[Fe II]})$], which shows a good agreement between them, with an average difference of $\Delta \log M_\bullet = \log M(\sigma_{[Fe II]}) - \log M(\sigma_\star) = 0.02 \pm 0.32$. In the same figure, we show also the masses for the SMBHs obtained for the subsample of unbarred galaxies as the open symbols, using equation (2), to obtain $\sigma_\star$. There is no difference in the average value of the SMBH masses obtained, and the mean scatter is 0.28 dex, which is somewhat smaller than the one for the complete sample.

6 CONCLUSIONS

We have used near-IR spectroscopic data of a sample of 47 active galaxies in order to investigate possible correlations between

the stellar velocity dispersion ($\sigma_\star$), obtained from the fit of the *K*-band CO absorption band heads, and the gas velocity dispersion (σ), obtained from the fit of the profiles of the [S III] $\lambda 0.95332\,\mu m$, [Fe II] $\lambda 1.25702\,\mu m$, [Fe II] $\lambda 1.644\,\mu m$ and $H_2\lambda 2.12182\,\mu m$ emission lines. The main conclusions of this paper are as follows:

(i) Very weak correlations are found between $\sigma_\star$ and both σ_{H_2} and $\sigma_{[S III]}$.

(ii) The best correlation is found for the [Fe II] emitting gas with $R = 0.58$ for the Spearman rank correlation coefficient between $\sigma_\star$ and $\sigma_{[Fe II]}$ (both $\lambda 1.257\,\mu m$ and $\lambda 1.644\,\mu m$ emission lines can be used). A better correlation is found if we exclude the barred galaxies from the sample ($R = 0.80$), while no correlation is found for the subsample of barred galaxies.

(iii) $\sigma_{[Fe II]}$ can thus be used to estimate $\sigma_\star$ for objects for which the stellar velocity dispersion cannot be measured or is unknown. The best fit of the data is given by the equation $\sigma_\star = 95.4 \pm 16.1 + (0.25 \pm 0.08) \times \sigma_{[Fe II]}$ for the complete sample and $\sigma_\star = 57.9 \pm 23.5 + (0.42 \pm 0.10) \times \sigma_{[Fe II]}$ for the subsample of unbarred galaxies.

(iv) The equations above should be improved and re-calibrated when larger and non-biased samples of near-IR spectra of AGNs become available.

(v) The scatter from a one-to-one relationship between $\sigma_\star$ and its value derived from $\sigma_{[Fe II]}$ using the equation above for our sample is 0.07 dex, which is smaller than the scatter of previous relations using $\sigma_{[O III]}$ in the optical as a proxy for $\sigma_\star$.

(vi) The use of $\sigma_{[Fe II]}$ in the near-IR instead of $\sigma_{[O III]}$ in the optical is particularly important for cases in which the optical spectra are not available or are obscured, as in the case of many AGNs.

(vii) The comparison of the masses for SMBHs obtained from the direct use of $\sigma_\star$ in the $M_\bullet$–$\sigma_\star$ relation with those using $\sigma_{[Fe II]}$ to obtain $\sigma_\star$ reveals only a small average difference of $\Delta \log M_\bullet = 0.02 \pm 0.32$ for the complete sample and $\Delta \log M_\bullet = 0.00 \pm 0.28$ excluding barred galaxies from the sample.

ACKNOWLEDGMENTS

REFERENCES

Booth C. M., Schaye J., 2011, MNRAS, 413, 1158
Bower R. G. et al., 2006, MNRAS, 370, 645
Cappellari M., Emsellem E., 2004, PASP, 116, 138
Crenshaw D. M., Kraemer S. B., 2007, ApJ, 659, 250
Crenshaw D. M., Kraemer S. B., Schmitt H. R., Kaastra J. S., Arav N., Gabel J. R., Korista K. T., 2009, ApJ, 698, 281
Crenshaw D. M., Kraemer S. B., Schmitt H. R., Jaffé Y. L., Deo R. P., Collins N. R., Fischer T. C., 2010, AJ, 139, 871
Das V., Crenshaw D. M., Kraemer S. B., 2007, ApJ, 656, 699
Das V. et al., 2005, AJ, 130, 945
Di Matteo T., Springel V., Hernquist L., 2005, Nat, 433, 604
Ferrarese L., Ford H. C., 2005, Space Sci. Rev., 116, 523
Ferrarese L., Merrit D., 2000, ApJ, 547, 140
Fischer T. C., Crenshaw D. M., Kraemer S. B., Schmitt H. R., Trippe M. L., 2010, AJ, 140, 577
Fischer T. C., Crenshaw D. M., Kraemer S. B., Schmitt H. R., Mushotsky R. F., Dunn J. P., 2011, ApJ, 727, 71
Gebhardt K. et al., 2000, ApJ, 539, 13
Graham A. W., Onken C. A., Athanassoula E., Combes F., 2011, MNRAS, 412, 2211
Greene J. E., Ho L. C., 2005, ApJ, 630, 122
Greene J. E., Ho L. C., 2006, ApJ, 641, L21
Jahnke K., Maccio A. V., 2011, ApJ, 734, 92
Kaspi S., Maoz D., Netzer H., Peterson B. M., Vestergaard M., Jannuzi B. T., 2005, ApJ, 629, 61
Kelly B. C., 2007, ApJ, 665, 1489
Magorrian J. et al., 1998, AJ, 115, 2285
Nelson C. H., Whittle M., 1996, ApJ, 465, 96
Nemmen R., Bower R., Babul A., Storchi-Bergmann T., 2007, MNRAS, 377, 1652
Onken C. A., Ferrarese L., Merritt D., Peterson B. M., Pogge R. W., Vestergaard M., Wandel A., 2004, ApJ, 615, 645
Paturel G., Petit C., Prugniel Ph., Theureau G., Rousseau J., Brouty M., Dubois P., Cambrésy L., 2003, A&A, 412, 45
Peterson B. M., 2008, New Astron. Rev., 52, 240
Richstone D. et al., 1998, Nat, 395, A14
Riffel R. A., 2010, Ap&SS, 327, 239
Riffel R. A., Storchi-Bergmann T., 2011a, MNRAS, 411, 469
Riffel R. A., Storchi-Bergmann T., 2011b, MNRAS, 417, 2752
Riffel R. A., Sorchi-Bergmann T., Winge C., Barbosa F. K. B., 2006a, MNRAS, 373, 2
Riffel R., Rodríguez-Ardila A., Pastoriza M. G., 2006b, A&A, 457, 61
Riffel R. A., Storchi-Bergmann T., Winge C., McGregor P. J., Beck T., Schmitt H., 2008, MNRAS, 385, 1129
Riffel R. A., Storchi-Bergmann T., Dors O. L., Winge C., 2009, MNRAS, 393, 378
Riffel R. A., Storchi-Bergmann T., Nagar N. M., 2010, MNRAS, 404, 166
Rodríguez-Ardila A., Pastoriza M. G., Viegas S. M., Sigut T. A. A., Pradham A. K., 2004, A&A, 425, 457
Rodríguez-Ardila A., Contini M., Viegas S. M., 2005, MNRAS, 357, 220
Salviander S., Shields G. A., Gebhardt K., Bonning E. W., 2006, New Astron. Rev., 50, 803
Springel V., Di Matteo T., Hernquist L., 2005, ApJ, 620, 79
Storchi-Bergmann T., McGregor P. Riffel, Rogemar A., Simões Lopes R., Beck T., Dopita M., 2009, MNRAS, 394, 1148
Storchi-Bergmann T., Simões Lopes R., McGregor P. Riffel, Rogemar A., Beck T., Martini P., 2010, MNRAS, 402, 819
Vestergaard M., Peterson B. M., 2006, ApJ, 641, 689
Winge C., Riffel, Rogemar A., Storchi-Bergmann T., 2009, ApJS, 185, 186
Wu Q., 2009, MNRAS, 398, 1905
Xiao T., Barth A. J., Greene J. E., Ho L. C., Bentz M. C., Ludwig R. R., Jiang Y., 2011, ApJ, 739, 28

This paper has been typeset from a TeX/LaTeX file prepared by the author.